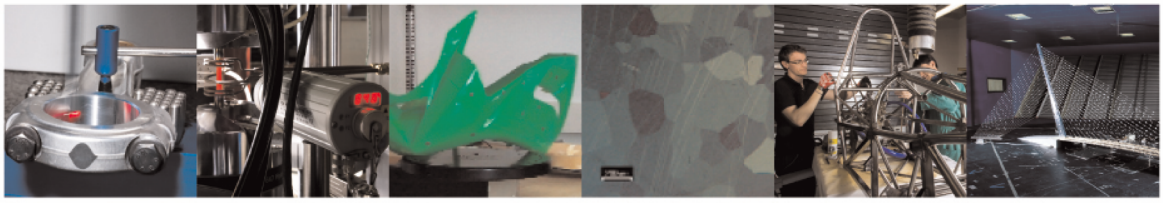

Experimental analysis of mode I crack propagation in adhesively bonded joints by optical backscatter reflectometry and comparison with digital image correlation

R.A.A. Lima, R. Perrone, M. Carboni, A. Bernasconi

This is a post-peer-review, pre-copyedit version of an article published in Theoretical and Applied Fracture Mechanics. The final authenticated version is available online at: https://doi.org/10.1016/j.tafmec.2021.103117

DIPARTIMENTO DI MECCANICA ■ POLITECNICO DI MILANO
via G. La Masa, 1 ■ 20156 Milano ■ EMAIL (PEC): pecmecc@cert.polimi.it
http://www.mecc.polimi.it
Rev. 0

Experimental analysis of mode I crack propagation in adhesively bonded joints by optical backscatter reflectometry and comparison with digital image correlation.

R. A. A. Lima, R. Perrone, M. Carboni, A. Bernasconi*

Department of Mechanical Engineering, Politecnico di Milano, Milano, Italy

The relationship between the response of backface strain distributed sensing by Optical Backscatter Reflectometry and the damage in the adhesive was studied using double cantilever beam specimens. Digital Image Correlation and visual inspection provided information about the crack-tip position and the extension of the cohesive process zone. The comparison between the features of the backface strain pattern and the position and size of the cohesive zone led to the conclusion that, for the studied adhesive, backface distributed sensing allows for the onset of plastic deformations ahead of the crack-tip to be identified, opening new perspectives for fatigue crack monitoring and in-service measurements.

Keywords: adhesive bonded joints, crack propagation, digital image correlation, optical backscatter reflectometry.

* Corresponding author. Email: andrea.bernasconi@polimi.it; Tel +39 02 2399 8222

1. INTRODUCTION

The use of adhesively bonded joints in aeronautical and automotive fields has grown significantly in recent years due to their high strength to weight ratio, design flexibility in multi-materials joints and more uniform stress distributions concerning mechanical joints. However, adhesive joints present a lack of long-term reliability because of environmental and mechanical degradations [1-5]. Consequently, to increase the in-service reliability and safety of adhesively bonded joints in primary structures, either a damage tolerant design [6] or a Structural Health Monitoring (SHM) approach [7,8] are, nowadays, being developed and implemented.

The damage tolerance philosophy assumes that any given structure contains defects able to propagate during its operational life. Therefore, in order to ensure in-service safety, this method requires the optimised definition of the periodicity ("inspection interval") of service interruptions for maintenance and the application of Non-Destructive Testing (NDT). To this aim, life predictions based on fracture mechanics concepts and the capability, i.e., the Probability of Detection, of the adopted NDT techniques must be available [6].

On the other hand, SHM is based on real-time, or on-demand, monitoring of the structural integrity of a component or structure during service, also called "diagnostics", and it is a key for the real-time estimation during service, also called "prognostics", of the "remaining useful life". To this aim, a reliable evaluation of the monitored damage (at least, its size and location), the permanent instrumentation of the monitored structure, and the application of Big Data analytics methods to the acquired data are needed [7-9].

Despite the above-mentioned conceptual and methodological differences between a damage tolerant design and SHM, both approaches rely on an accurate assessment of damage size and its location, particularly in the case of adhesively bonded joints. From this perspective, it is worth remarking that the in-service structural integrity of adhesively bonded joints can be affected by damage (i.e. crack) initiation and propagation. That can be a consequence of either the presence of manufacturing defects (such as voids, kissing

bonds and inclusions among many others) or in-service loading conditions (such as fatigue or impacts) or both simultaneously, by the geometry of the joint and by the material of the substrates [1].

Composite bonded joints can fail in the substrate (i.e., fibre-tear breaking, delamination, and stock-break failure), in the substrate/adhesive interface (adhesive failure), or the adhesive layer (cohesive failure). On the other hand, metallic adhesively bonded joints mainly undergo adhesive and/or cohesive failures [10]. This work aims at testing the capability of a distributed backface strain sensing method to monitor the crack propagation in the bondline. Therefore, metallic substrates were chosen to exclude all the above-mentioned damage mechanisms typical of composite joints, which might have hampered the interpretation of results.

The backface strain measurement is widely reported in the literature [5,11,14]. The traditional version of this method uses a discrete array of punctual strain sensors such as, for example, conventional strain gauges fixed on the external surface of one or both substrates of the adhesive joint. Once a crack in the adhesive propagates, the stiffness of the joint and its strain response change. Therefore, variations in the backface strain pattern of the adhesive joint are assessed by the sensors, and the crack-tip position can be inferred. The main advantage of backface strain measurement consists of the possibility of being used as an in-service damage monitoring method both in static and dynamic loading conditions and can be applied regardless of the type of substrate material. On the other hand, discrete sensing provides valuable information just in the regions of the joint close to and around the applied punctual sensors [15,16].

For this reason, other kinds of sensors are being studied, developed, and proposed. Several types of research investigated the performance of optical fibres as strain sensors in the backface strain measuring method. They present greater accuracy, long-term stability, and reduced sizes, providing less invasiveness in the system when compared to strain gauges or piezoelectric transducers [17-19]. The main types of adopted fibre optic strain sensors are Fibre Bragg Gratings (FBG) and Chirped Fibre Bragg Gratings (CFBG). Both measure the strain over the length of a Bragg grating. FBGs have a constant modulation period of

the refractive index, which enables measuring uniform strains over the sensor's length like a strain gauge [18]. In contrast, the period of CFBG varies linearly, thus enabling short length (limited to the Bragg gratings size) distributed sensing. Distributed sensing over a longer length can be achieved by Optical Backscatter Reflectometry (OBR) [20].

The OBR technique uses swept wavelength interferometry (a narrow band signal launched into the optical fibre by a low-power laser) to measure the Rayleigh backscattering caused by the intrinsic defects present in the core of the optical fibre and producing stochastic local modifications in the refractive index profile along its whole length. These random disturbances produce a unique Rayleigh backscatter profile representing a fingerprint of the whole given fibre. In addition, external temperature and/or strain stimuli produce changes of the optical fibre refractive index and, consequently, spectral and the local temporal Rayleigh backscattered profiles [21,22]. From these changes of the Rayleigh local patterns, and after suitable calibration, mechanical and thermal strains can be derived and measured. Since the reflectometer gathers a point-by-point response from the fibre, strain measurements are distributed. The spatial resolution of this method is of a virtual kind, i.e., a virtual gage length is set by the user depending on the needs and can vary from fractions of millimetres to kilometres.

Although many researchers [20, 23-25] have already studied backface strain measurement by optical fibres, distributed strain sensing by OBR has not been fully explored as a backface strain monitoring method yet. An application of OBR to monitor crack growth in a double cantilever beam (DCB) specimen can be found in [26] for the case of hybrid co-cured metal-CFRP specimens. In the present paper, a similar approach is applied to mode I, quasi-static crack propagation in an adhesively bonded DCB with metal adherents. The present work aims to interpret the relationship between the backface strain profile measured by OBR and the essential features of a crack developing in the bondline of adhesively bonded joints, which still presents open points. To achieve this goal, in the present research, the distributed backface strain measurements along optical fibres provided by OBR are discussed based on visual inspections and strain distributions measured in the bondline by Digital Image Correlations (DIC).

Considering the application of experimental stress/strain analysis approaches to bonded joints, numerous research projects used Digital Image Correlation (DIC) to measure crack size, crack tip location, and determine adhesives' cohesive properties [27-37].

As highlighted by Gorman *et al.* [31] and Reiner *et al*. [32], DIC can be a very accurate method to determine the energy release rate and the traction separation law of the adhesive joints in Double Cantilever Beam (DCB) tests. In addition, this method can give important information about the strain profile of the specimens. However, DIC can hardly be applied as an in-service monitoring technique because of the bulky equipment (out of the lab, for parts with non-planar surfaces, a 3D system is required) and the strict calibration requirements and complex procedures needed to obtain accurate measurements.

In this work, DIC was not used to determine the fracture properties of the studied adhesive like in [30-32], but as a validation tool for OBR results. OBR appears to be a promising technique for estimating the crack front position and the size of the process zone in the bondline of adhesive joints, particularly under fatigue loading. The present work is focused on the use of the backface OBR methodology to determine the strain profile of cracked adhesively bonded joints and to evaluate the relationship between the OBR response and the actual features of the present damage. A well-defined experimental case of study (quasi-static DCB test, i.e., an effective representative of mode I loading) is chosen to act in a more controlled and known scenario. OBR results are then compared and discussed with respect to DIC and visual inspection ones.

2. METHODS

2.1. Materials

DCB specimens were manufactured with high-strength steel DIN 40CrMoMn7 adherents bonded using a bi-component 3M Scotch-Weld^{TM} 7260 B/A (Non – Sag) epoxy adhesive. The mechanical properties of the adhesive and the steel adherends are reported in Tables 1 and 2.

Table 1: Mechanical properties of the adhesive 3M Scotch-Weld™ 7260 B/A [38]

Young's Modulus (MPa)	4248 ± 297
Ultimate stress (MPa)	40.6 ± 1.5
Poisson's ratio	0.35

Table 2: Mechanical properties of steel adherents [39].

Ultimate tensile strength (MPa)	1000
Yield stress (MPa)	861
Elongation at fracture (%)	14-17
Young's modulus – E (MPa)	205000

2.2. Sample's fabrication and preparation

Standard DCB specimens were manufactured according to ASTM D3433 [40], having length L = 290 mm, width w = 25 mm and thickness t = 12.5 mm. Before bonding, the substrates were sandblasted until the surface was evenly rough and then cleaned with acetone. The adhesive was mixed using a mixing nozzle for bi-component structural adhesives with the aid of a hydraulic applicator. Glass microspheres (concentration of 2% by adhesive weight), with 300 μm average diameter, were added to the adhesive to ensure a uniform adhesive layer thickness. A 0.15 mm thick Teflon patch was applied to both adherends to ensure a length of the starting notch a_0 of 50 mm. The polymerisation process was done in an oven by applying a linearly increasing temperature ramp from room

temperature up to 65°C in 1.5 hours, holding 65°C for 3 hours and descending to room temperature in 1 hour. Two specimens equipped with optical fibres were manufactured. They are here identified as S1 and S2. Five other specimens were manufactured and tested without optical fibres and results are reported in [39].

2.2.1. Optical fibres – bonding process

To measure backface strains, high-definition optical fibres equipped with LC/APC connectors were bonded on the external surface of the substrates by the following steps:

- the surfaces were slightly abraded with fine sandpaper (120 grit);
- surfaces were cleaned firstly with acetone and then with RMS1 (a chemical cleaning agent used in strain gauges bonding procedure);
- fibres were positioned and kept straight with adhesive tape for the bonding process;
- the X60 bi-component epoxy adhesive (supplied by HBM Company, Germany) was applied at room temperature with a curing time of 10 minutes.

Two different fibres' configurations were chosen, as shown in Fig. 1 (a). The specimen named S1 presented three parallel optical fibre paths applied to the same surface of the sample, while the one named S2 had one single path applied to both surfaces (top and bottom) of the specimen. The configuration with three paths bonded on the same side of the substrate was chosen to check if the method can detect a curved crack propagation front. With a single central path on both substrates, the second configuration was chosen to check if backface strain profiles on the two sides of the DCB specimen differ.

2.2.2. Digital Image Correlation – surface preparation

For Digital Image Correlation, a fine speckle pattern was painted on the lateral surface of the specimens to create a uniformly random textured pattern, Fig. 1 (b).

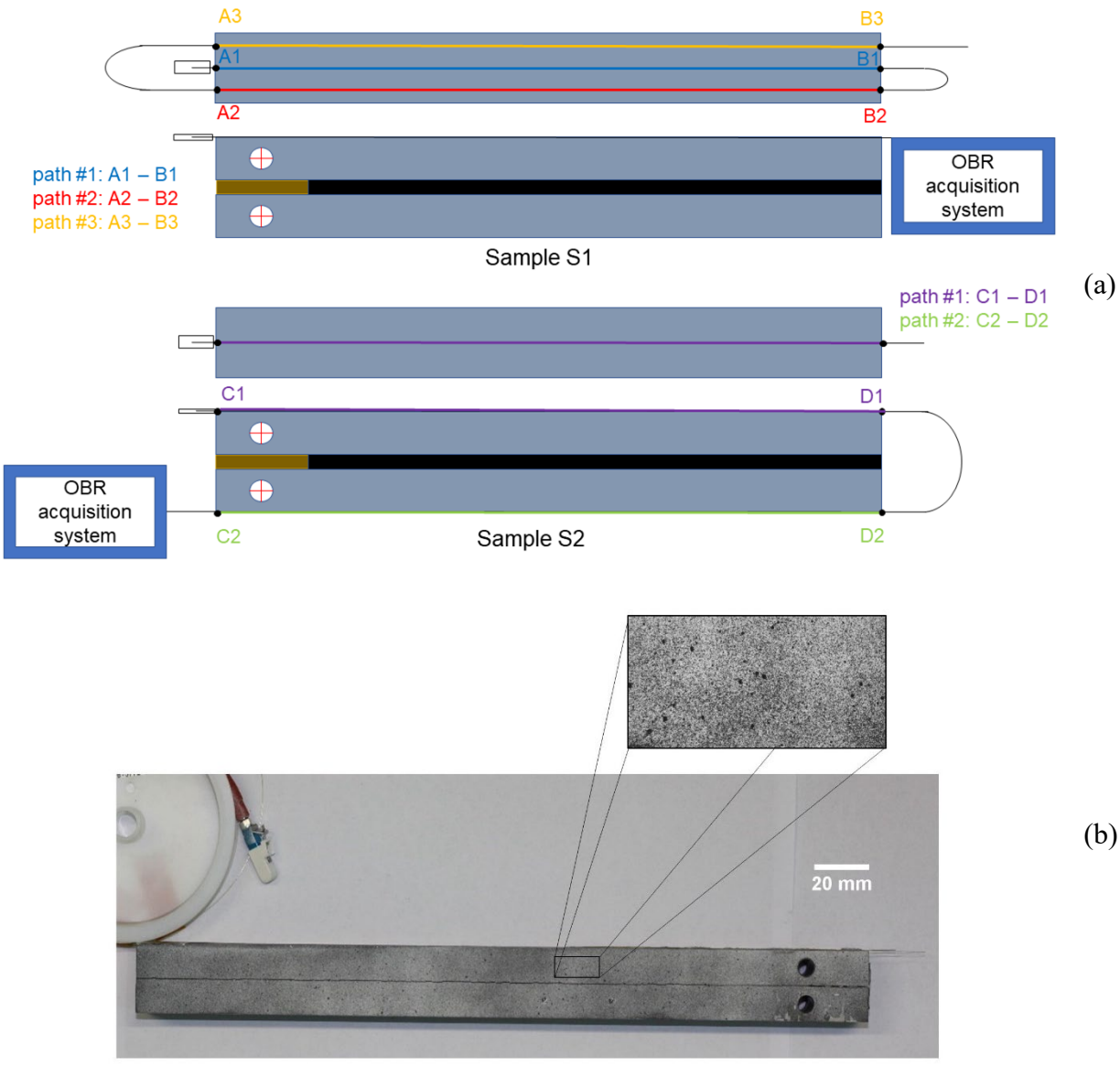

Figure 1: (a) Scheme of optical fibre application; (b) Sample with speckle pattern.

The speckle pattern was obtained by applying a first thin layer of white water-based painting followed by a random aerosol application of black painting.

2.3. DCB test procedures

DCB tests were performed using an MTS electro-mechanical testing machine with a 100 kN maximum capacity load cell. The system is equipped with a calibrated load cell rated class 0.5 according to ISO 7500-1 for loads greater than 1 kN, i.e., it has 0.5% accuracy of load measurements. As suggested by the ISO 25217 standard [41], a 0.5 mm/min test speed rate was used. The load (P) and the machine's crosshead displacement (δ) were recorded during each test.

For all DCB samples, a pre-cracking stage was performed, according to ISO 25217 [41], to ensure consistency with results reported in [39]. A quasi-static pure mode I load was applied for the pre-cracking stage with the same test speed used during the main test. When the maximum load was achieved and a drop in the measured load was observed, the specimen was unloaded. After complete unloading, the testing stage started.

2.3.1. Backface strain measurement setup

To measure and record backface strains during DCB tests, the optical fibres were connected to an OBR ODiSI-B interrogator from Luna Innovations Inc. (Roanoke, Virginia, USA). The OBR interrogator acquires and processes the Rayleigh backscatter radiation profile and transforms it into a strain profile. The entire fibre was used as a distributed sensing unit with a high-space resolution in the order of millimetres. Specifically, virtual sensors, having a virtual gauge length of 1.3 mm, were specified over discrete portions of the fibre and used to calculate single strain measurements. The gauge pitch, i.e., the length of fibre between the centres of a single gage and its nearest neighbour, was set to 0.65 mm. The OBR interrogator acquired data at 5 Hz with a resolution of 1 με. Before the DCB test started, the acquired signal obtained by the OBR system were tared with consideration to the temperature of the laboratory and residual strain conditions.

2.3.2. DIC measurement setup

The 3D ARAMIS Adjustable system by GOM was used for measuring the displacement field on the lateral surface of each DCB specimen. The system includes two adjustable 12 Megapixels cameras, dual-LED lighting, and post-processing software. The calibration process of the DIC system was done using a calibration panel (CP 40/MV) at a specific stand-off distance of 697 mm (recommended for the selected measuring volume). During this procedure, temperature and image distortions were adjusted. In the end, a calibration deviation of around 0.03 pixels was found. The DIC hardware and analysis parameters are reported in Tables 3 and 4.

Table 3: DIC hardware parameters.

Camera	ARAMIS Adjustable 12 M
Image resolution	4096 x 3000 pixels
Lens	Titanar B 75 mm
Aperture	22
Field-of-view	110 mm
Image scale	39 pixels / mm
Stereo-angle	25 degrees
Stand-off distance	697 mm
Measuring volume	110 x 80 x 80 [m^3]
Dual LED	10°
Image acquisition rate	1 Hz – sample S1 2 Hz – sample S2

Table 4: DIC analysis parameters.

DIC software	GOM Correlate 2018
Image filtering	No filters were used
Subset size	33 pixels
Step size	11 pixels
Matching criterion	Cross-correlation against definition stage
Interpolant	Bilinear spline

2.3.3. Visual crack length estimation

The visual estimation of crack length during the tests was performed, as suggested by ISO 25217 [40], by taking pictures via the Aramis adjustable system and an acquisition frequency of 1 Hz and 2 Hz for specimens S1 and S2, respectively. The camera setup could synchronise each picture frame with the related load and displacement values retrieved from the testing machine.

For each specimen, about 20 representative frames were then considered for crack length estimation using the GOM correlating software supplied with the Aramis adjustable system. In each frame, two points were manually picked (Fig. 2): a reference point (Point 1) related to the end of the Teflon tape, which is the same distinguishable mark for all the considered frames, and the crack tip position (Point 2). The distance measurement tool of the calibrated GOM correlating software was then used to measure the crack length in each selected frame.

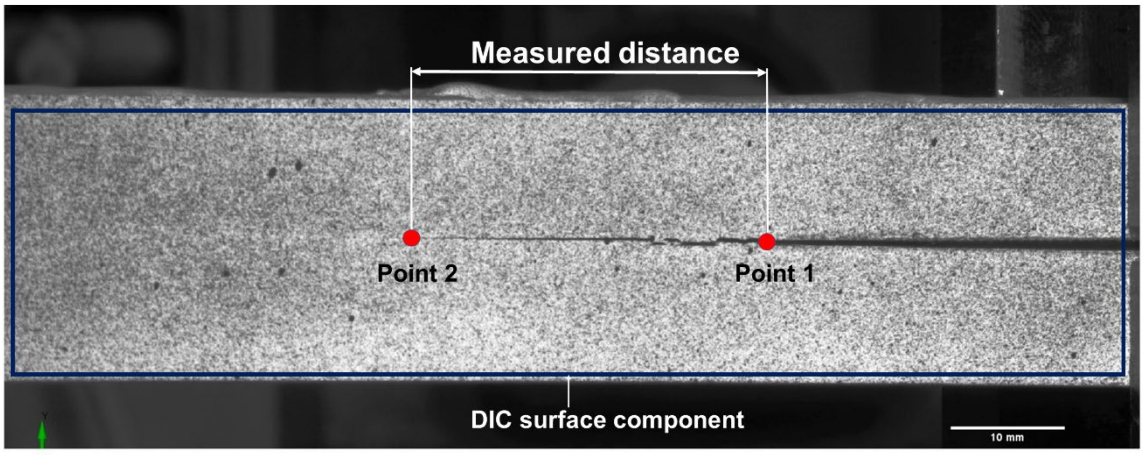

Figure 2: Visual evaluation of the crack length was determined through manual selection of measurement points.

3. RESULTS AND DISCUSSION

3.1. DCB test results

The complete load versus crosshead displacement curves for both specimens are shown in Fig. 3.

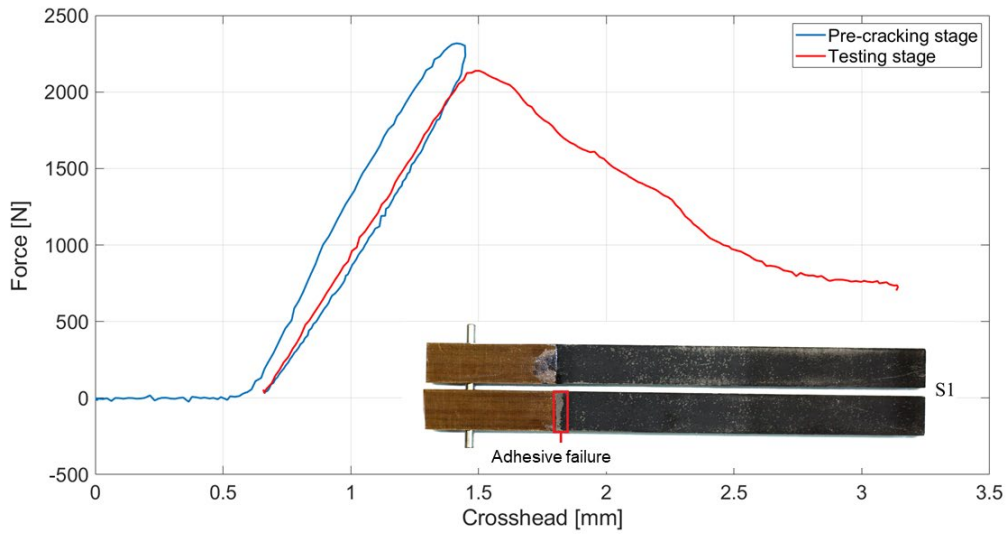

(a)

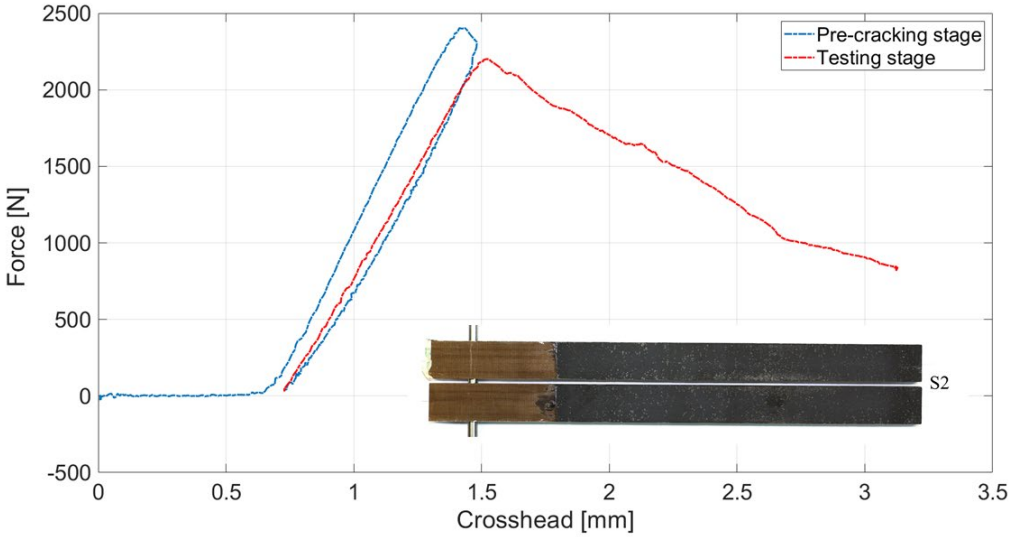

(b)

Figure 3: Load vs displacement of pre-cracking and testing stages – (a) specimen S1 and (b) specimen S2.

As can be seen in Figure 3, the two specimens presented similar load-displacement curves. The blue curves represent the pre-cracking stage performed to ensure a sharp crack tip

within the bondline. The red curves represent the quasi-static mode I testing stage and the crack propagation during the test.

Results agreed with five other tests reported in [39]. On the fracture surface of specimen S1, an initial adhesive failure was identified close to the Teflon patch, which presumably took place during the pre-cracking stage, as shown in the detail of Figure 3 (a). Specimen S2 showed a cohesive failure, Figure 3 (b).

3.2. Crack length estimation by visual inspection

After the measurements, a load vs estimated (by visual inspection) crack length graph was drawn, as can be seen in Fig. 4.

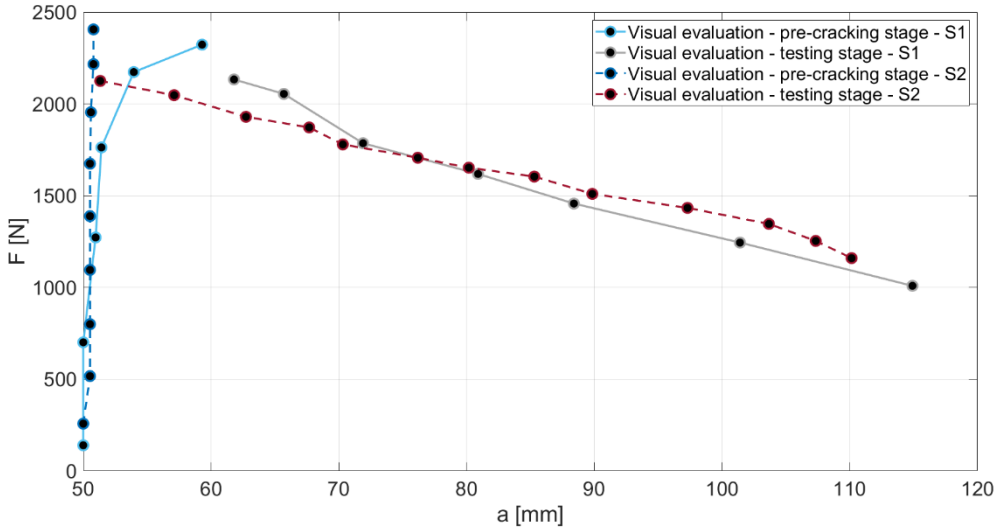

Figure 4: Load vs crack length by visual evaluation.

The visual evaluation curves are divided into pre-cracking and testing stages. During the pre-cracking stage, it is possible to notice that the specimens behaved differently. The visually estimated crack length after the pre-cracking stage was about 59 mm and 51 mm for S1 and S2, respectively. Sample S1 presents more significant increments in the adhesive's crack length at the last steps of the pre-cracking stage (from 1500 N to the

maximum load – about 8 mm of propagation) against an almost negligible crack length increment in the sample S2. This difference might also be explained by the adhesive failure mechanism observed in specimen S1, see Section 3.1.

3.3. OBR measurements

In general, the backface strain profile generated by the applied loads over the surface of adhesively bonded specimens displays a characteristic peak strain associated with the position of the crack tip in the adhesive [14, 24, 42]. The DCB specimens studied in this work displayed the backface strain pattern measured by OBR shown in Figure 5 for specimen S1. As both specimens presented similar results, only the results of sample S1 are presented in this section.

Sample S1 presents three optical fibre paths bonded on the back face of one of the two substrates (Fig. 1a). The exemplificative optical fibre strain profile distribution at 1762 N as a function of the optical fibre length is represented in Fig. 5.

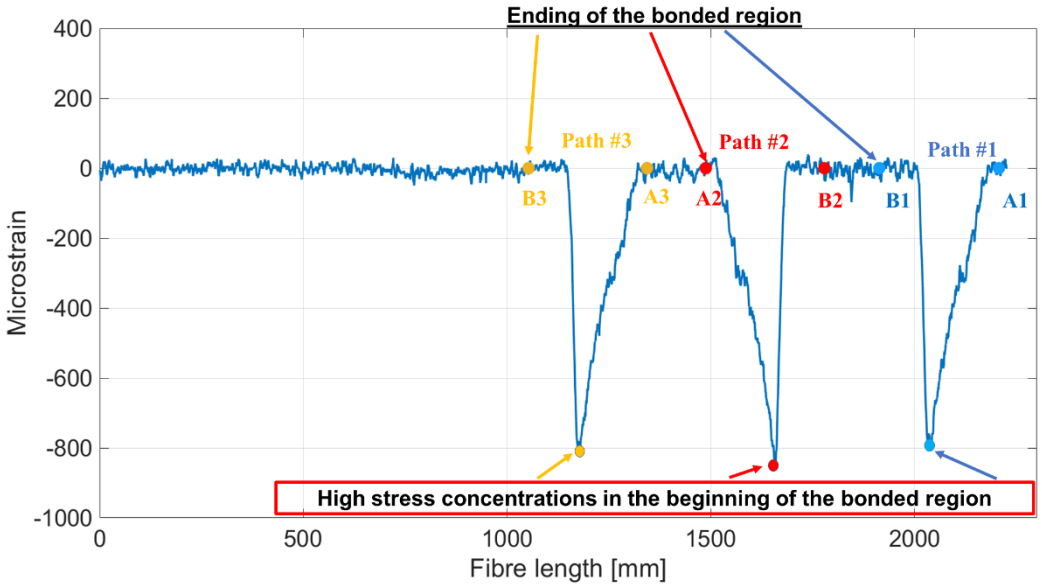

Figure 5: Optical fibre strain distribution at 1762 N (sample S1).

As the optical fibre length was known, it was possible to determine the position of specific points of interest. So, the beginning and end of the bonded paths on the back face of the specimens were identified using a localised heat source (optical fibres are also sensitive to changes in temperature, not only in mechanical strains) that, once placed close to the fibre, caused an alteration in the OBR pattern. So, the beginning (A1, A2 and A3) and end spots of the optical fibres bonded paths (B1, B2 and B3) were identified.

As can be observed, the strain distribution of the optical fibre presents three symmetrical curves associated with each path. Thus, along with paths #1 and #3, the signal travels through the fibre from the unloaded extremity of the specimen (B1 and B3) to the loaded one (A1 and A2), while path #2 is the opposite.

The maximum strain peak observed at this point of the test was about 800 με and can be associated with the beginning of the bonded region, according to Saha *et al.* [43].

Figure 6 (a) and (b) show the exemplificative evolution of the acquired signals during the pre-cracking and the testing stages for path #2, respectively (strain profiles were rectified, i.e. made positive).

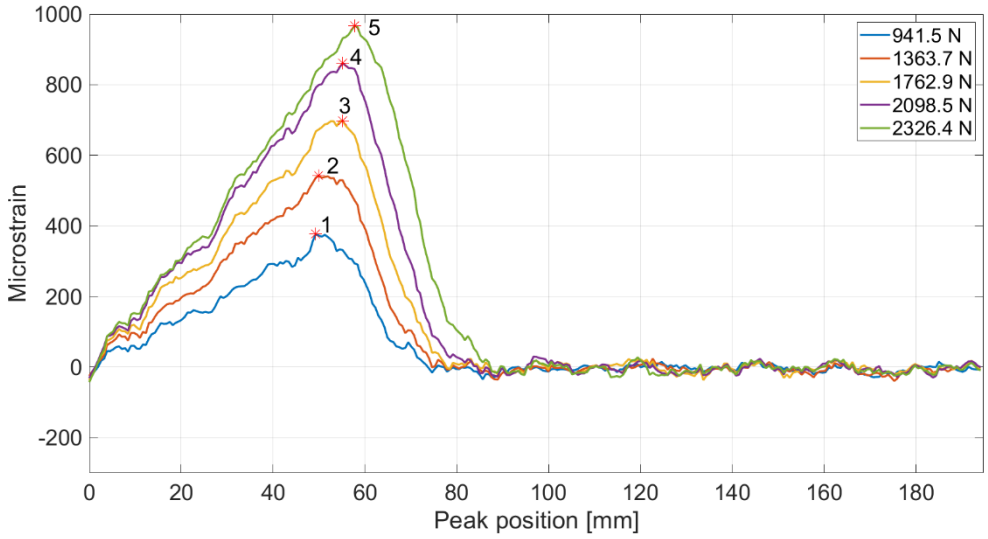

(a)

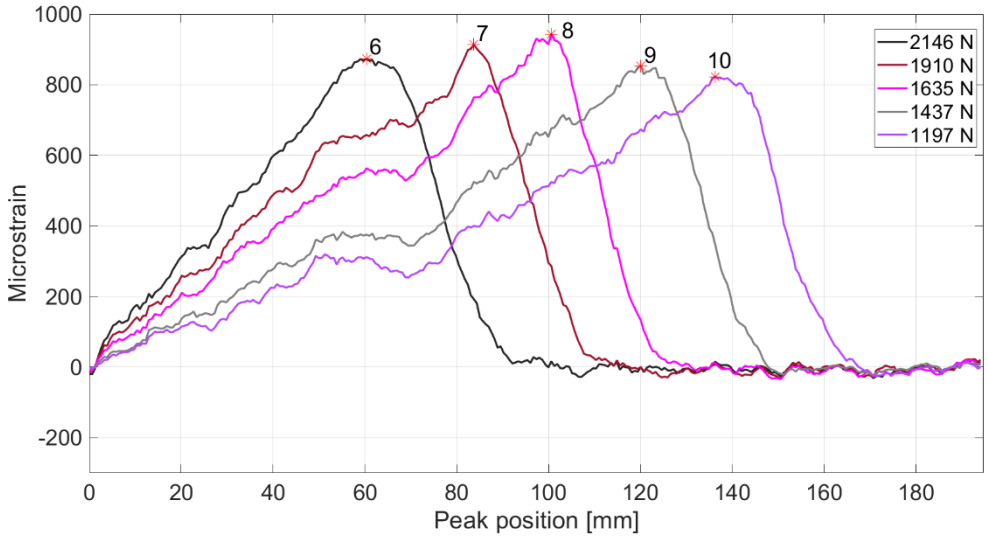

(b)

Figure 6: Peak strain as a function of its position on the specimen length (path #2): (a) pre-cracking stage and (b) testing stage.

Each curve represents the strain profile recorded at a specific load level reached during the test. As can be seen in Figure 6 (a) for the pre-cracking stage, the peak strain started to grow, keeping the same position up to 1400 N. Then, when the load exceeded 1400 N, a

shift of the strain peak position was observed, and it could be related to crack propagation during the pre-cracking stage.

Figure 6 (b) showcases the strain profile of the optical fibre during the testing stage. When the maximum load was reached (curve 6), the crack started to propagate again, and the peak position shifted accordingly. In contrast, the absolute value of the strain peak remained almost constant (in the interval between 850 and 950 με). The same behaviour was found along the other fibre paths (paths #1 and #3).

The peak position of path #2 as a function of the applied load during the pre-cracking and testing stage can be observed in Figure 7. As already discussed, the peak position during the pre-cracking stage maintains almost the same position until 1400 N, and then it moves from the initial position ($a_0 = 50\,mm$) to 58 mm as it reaches the maximum load of the pre-cracking. During the testing stage, the assessed peak position further increases as the crack propagates.

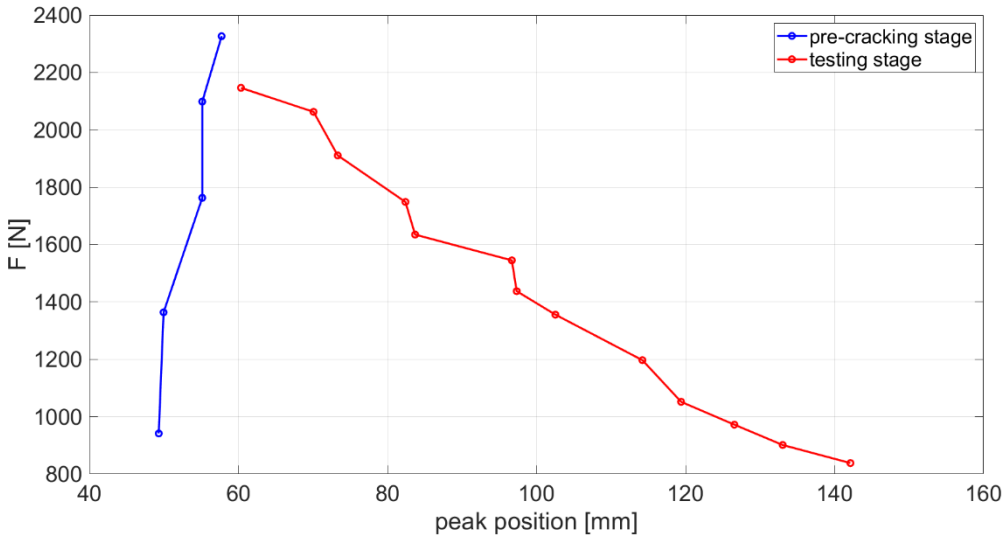

Figure 7: Load vs peak position of path #2 during the pre-cracking and testing stage.

3.4. DIC measurements

The DIC setup was synchronised with the load and displacement outputs from the testing machine, allowing the correlation between them and the picture frames taken during the test (about 700 frames for each test). The images present a resolution of 1 pixel equal to 3.45 μm.

DIC post-processing stage was performed using the GOM Correlate software. As shown in Table 4, a subset of 33 pixels and a distance of 11 pixels between each subset centre were chosen. A Region Of Interest (ROI) was selected, and a colour-coded map was created, for each frame, correlating the variations in the DCB vertical displacement fields. Figure 8 shows sample S1 vertical displacement map under 780.5 N (frame 220).

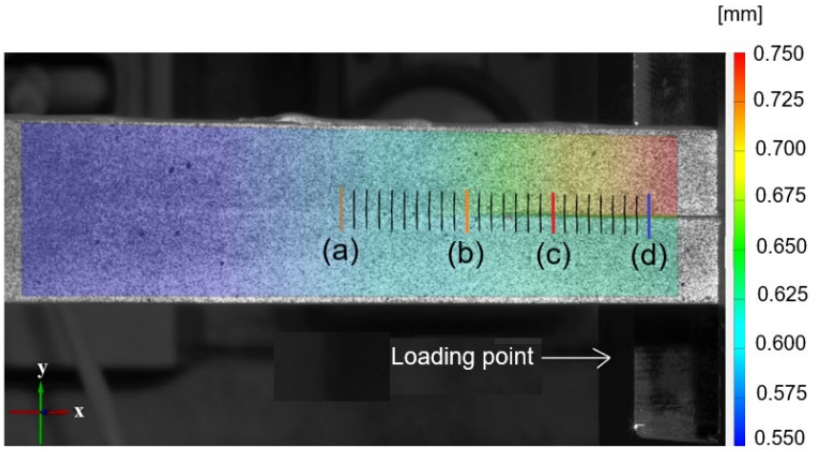

Figure 8: Vertical displacement measurements in the specimen's surface of sample S1 at frame 220 (780.5 N).

The displacement field coloured map created by the correlation software does not give enough information for the crack-tip localisation and, consequently, the estimation of crack length. Moreover, the resolution of the DIC system does not allow for the local strains in the adhesive to be measured accurately. Therefore, the method proposed in [44] to identify the crack tip position in composites DCB was applied. This method identifies the position

of the crack tip as the point of transition between two zones, the first characterised by constant relative displacement between the adherents and the second characterised by variable displacement.

To illustrate how this method can be applied to adhesively bonded joints, an analysis of the displacement field along vertical lines (y-direction), drawn across the bondline, forming a grid of lines horizontally spaced (x-direction) by 2 mm, is presented in Fig. 8. First, the relative vertical displacement along lines was determined using a function of the GOM correlate software, which allows for the displacement values along selected reference lines to be extracted from the measured displacement field. The relative displacements were then evaluated by analysing the extracted data. This analysis of the vertical displacements also allowed for the strains in the bondline to be inferred, as discussed in the following paragraphs.

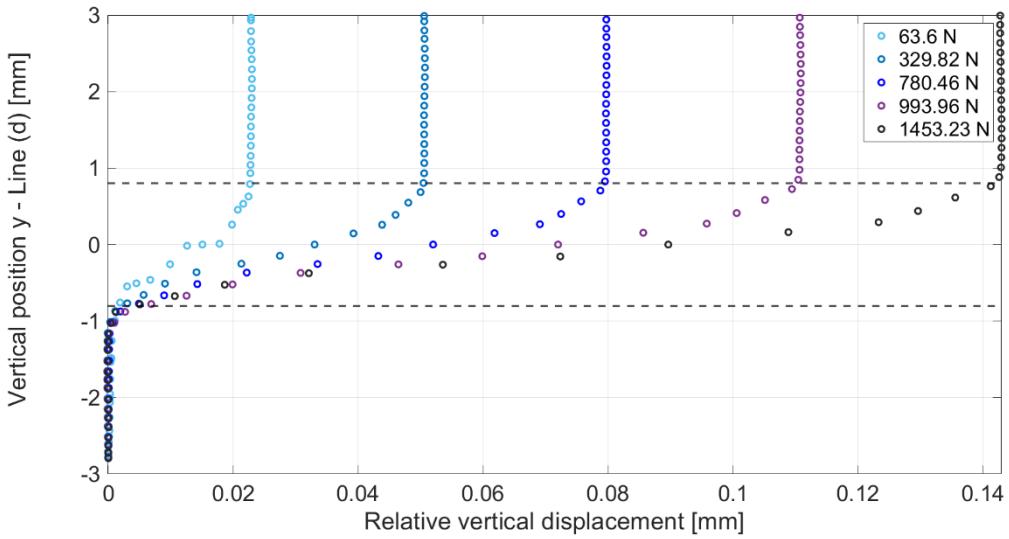

Figure 9: Relative vertical displacement along the line (d) of Figure 8 at different load levels.

Figure 9 showcases the vertical displacements data along the line segment (d) of Figure 8 in different loading conditions. The relative displacements are constant through the

thickness of the substrates. This corresponds to an almost rigid displacement of the points belonging to the substrates, far from the bondline. Non-null relative displacements are recorded only across the bondline, in the region indicated by two parallel dashed lines in Figure 9.

The 2 mm wide region between the black dashed lines of Figure 9 does not correspond to the thickness of the adhesive (0.3 mm). Gorman et al. 2019 [31] stated that this extended transition region could be related to the measurement noise effect that depends on the subset size choice and the cameras' resolution. However, the displacements evaluated outside the dashed region can be accurately measured since the much higher elastic modulus of the metallic substrates ensures minimal strain effects on their surface.

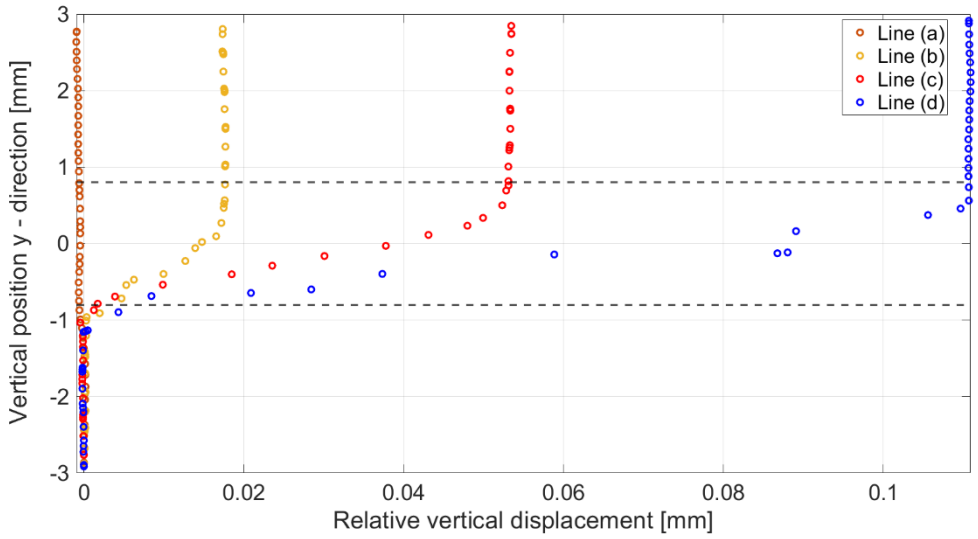

Figure 10: Relative vertical displacement along lines (a), (b), (c) and (d) of Figure 8 at frame 220 (780.5 N).

Figure 10 showcases the relative vertical displacement of the lines (a), (b), (c) and (d) of Figure 8 at frame 220 (applied load of 780.5 N). Line (a), located at the farthest distance from the loading pins, presents almost zero values of relative vertical displacement. On the left of line (a), similar small values of relative displacement can be found, allowing for a

zone of constant displacement to be identified. Displacement along lines (b), (c) and (d) are increasing with the distance from line (a). The zone on the right of line (a) corresponds to what is defined in [44] as a "variable displacement zone".

According to [44], the point representing the transition from the constant displacement zone to the variable displacement zone can be associated with the crack-tip. The transition point is identified as the point where relative displacements exceed a threshold defined based on the standard deviation of the displacements along the vertical line segments of the constant displacement zone. Relative displacements across the bondline far from the crack tip, on the side opposite to the loading pins, due to the typical noise of DIC measurements and to the presence of a deformable layer of adhesive (the latter do not present in [44]), are small, but not null. Figure 11 showcases the standard deviation values of the relative displacement measured along each vertical line of the grid.

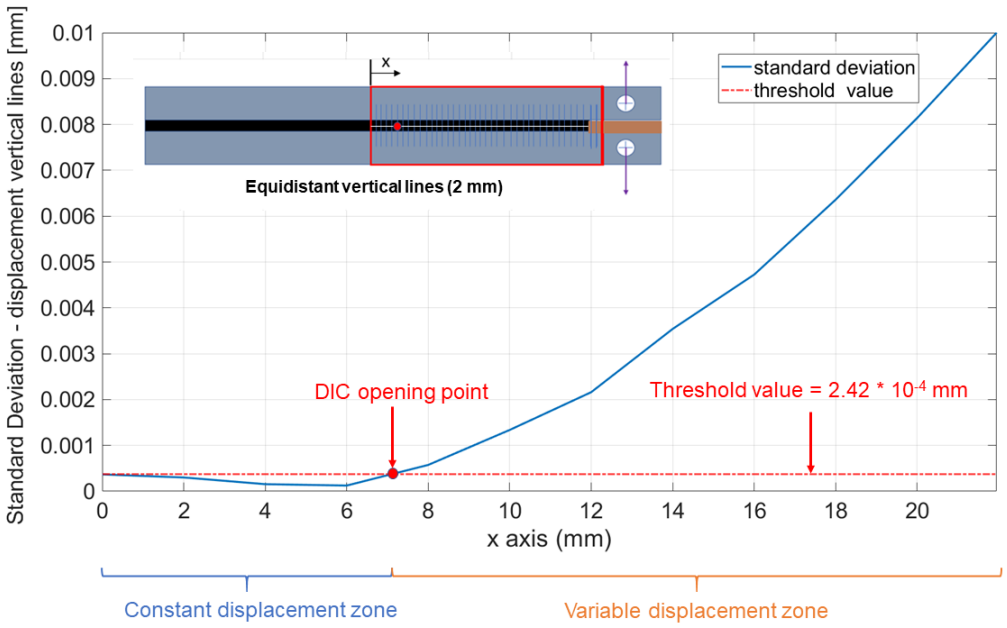

Figure 11: Standard deviation of the relative vertical displacement along all the lines created at frame 220 of sample S1 (780.5 N).

In Figure 11, it is possible to identify an almost constant standard deviation zone with slight fluctuations in the proximity of the crack opening. These variations can be associated with the slight rotation that the samples undergo during the test producing compressive effects in the region near the crack-tip [44]. This zone corresponds to the constant displacement zone. The maximum value of the standard deviation in this zone defines the threshold used to identify the crack tip in [44]. Here, to differentiate this point from the crack tip identified by visual inspection, this point will be indicated as "DIC opening point".

The analysis of the displacement values along all the line segments of Figure 8 is time-consuming. The absence of relative displacements along y-direction within the adherents allows for a more efficient evaluation of the relative displacements through the bondline to be obtained using the virtual extensometers defined in GOM software. These virtual extensometers can be automatically created along two parallel horizontal lines, and relative displacements can be extracted with low computational effort. Relative displacements were measured by a grid of equally spaced virtual extensometers defined with a step of 0.25 mm and a total length of 6 mm.

In order to interpret the transition between constant and variable displacement zones (DIC opening point) in terms of damage in the adhesive, strains in the bondline were inferred from relative displacements between the adherents. The strains (in the y-direction) in the bondline were calculated by dividing the relative vertical displacement by the bondline thickness. Since the elastic modulus of the substrates is more than forty times larger than that of the adhesive, the relative displacement can be ascribed entirely to the adhesive layer. Thus, the transverse strain evaluated at the position of the DIC opening point is equal to 1%. The 3M 7260 B/A bulk specimens displayed an elastic behaviour up to 1% strain and then an almost perfectly plastic behaviour up to 7%, the ultimate strain at failure [38]. Therefore, the point identified as the DIC opening point can be related to the onset of the plastic behaviour in the adhesive and not to the crack tip, as it was in [44] for the delamination of composite DCB specimens.

Figure 12 showcases the comparison between the position of the DIC opening points and the crack-tip position identified by the visual evaluation versus the load during the pre-

cracking and testing stage of specimen S1. During crack initiation, at the beginning, the DIC senses the opening of the arms of the DCB specimen behind the crack tip, whose position is fixed and determined by the Teflon patch. Therefore, the DIC opening point is placed behind the crack tip. Then, when the crack starts propagating, the DIC opening point passes over the crack tip and then stays in front of the crack tip until the end of the pre-cracking stage. Here, the two-point almost coincide, most probably because of the adhesive failure reported in Figure 3a. During the following testing stage, similar behaviour can be observed, but in this case, where the propagation is cohesive, the position of the DIC opening point is always in front of the crack-tip position determined by visual evaluation. When the failure is cohesive, the distance between the DIC opening point and the crack tip identified by visual evaluation can be interpreted as the length of the process zone [45], as depicted schematically in Figure 13. For the case at hand, this distance remained almost constant and around 10 mm during the tests.

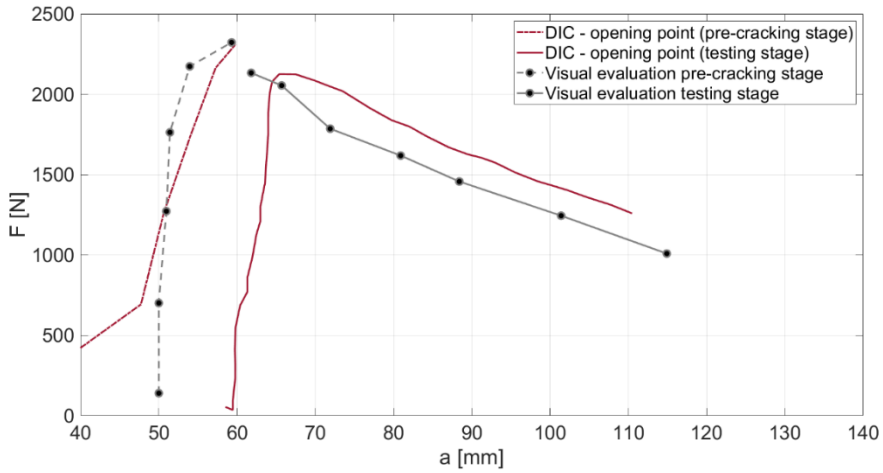

Figure 12: Comparison between crack-tip position determined by the visual evaluation and DIC opening point, corresponding to 1% of strain in the adhesive, as a function of the testing load in the pre-cracking and testing stages for specimen S1.

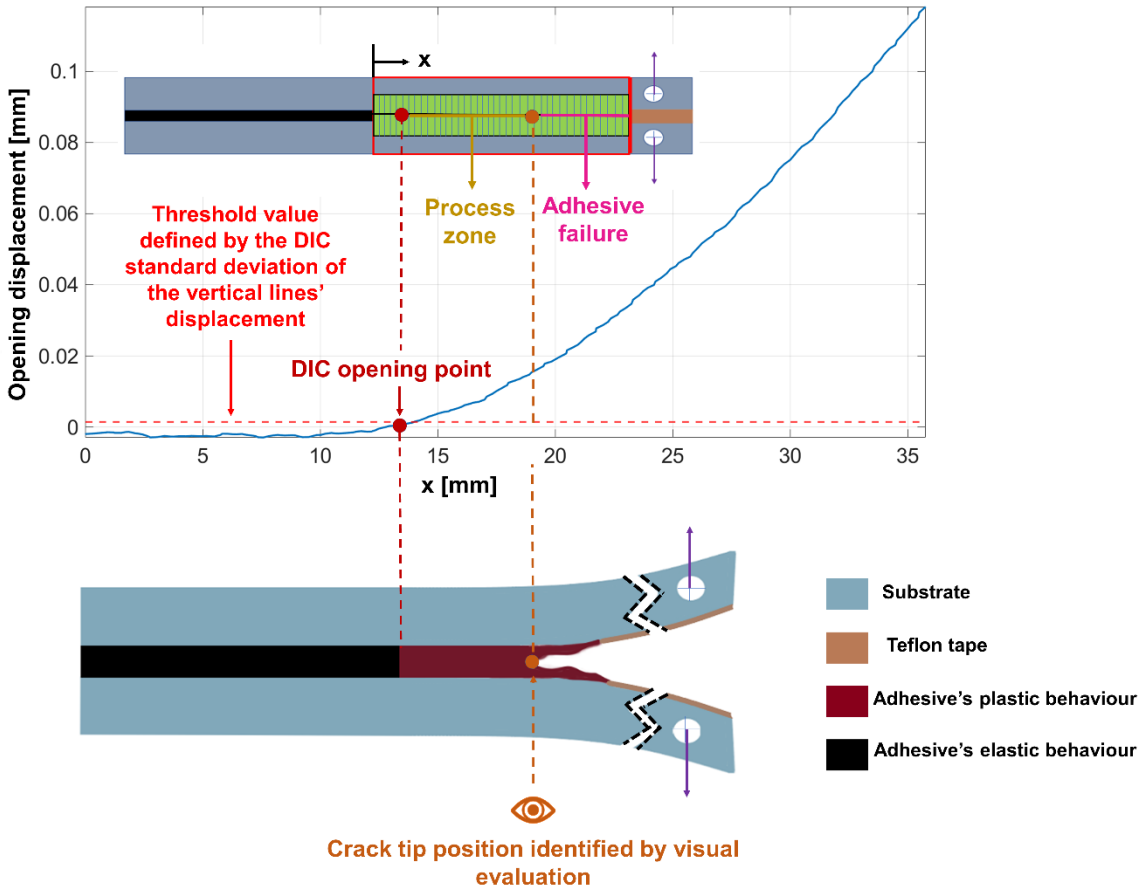

Figure 13: DIC opening POINT and its association with the onset of plasticisation of the adhesive instead of the crack-tip position within the adhesive – illustrative scheme.

The analysis based on DIC allowed for the onset of plasticisation within the adhesive to be identified, a position which can hardly be identified by the visual evaluation method. On the other hand, this method cannot be used in service life measurements due to the already mentioned bulky equipment and calibration requirements. OBR and fibre optic sensors are believed to be more versatile for in-service life measurements. Therefore, it is interesting to study the relationship between what was observed visually and measured by DIC and the characteristic features of the strain profile recorded by OBR.

3.4.1. Comparison of OBR to the other experimental techniques

A comparison between the crack length inferred by visual inspection, the location of the onset of plasticity (DIC opening point), and the position of the strain peak recorded by OBR as a function of the applied load during the pre-cracking and the testing stages is presented in Figures 14 and 15 for specimens S1 and S2, respectively.

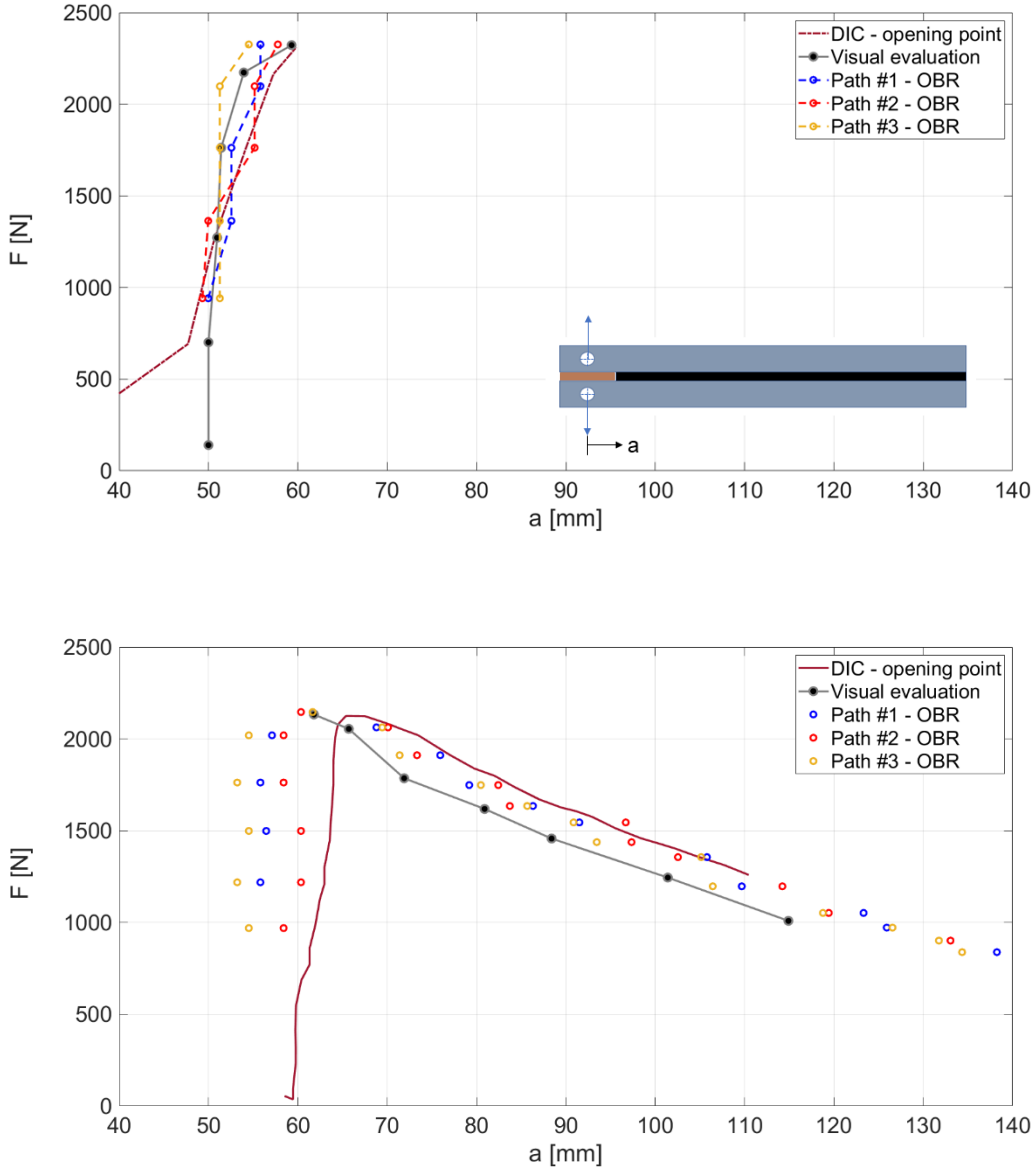

Figure 14: Comparison between the results obtained by the different techniques during (a) pre-cracking and (b) testing stage - specimen S1.

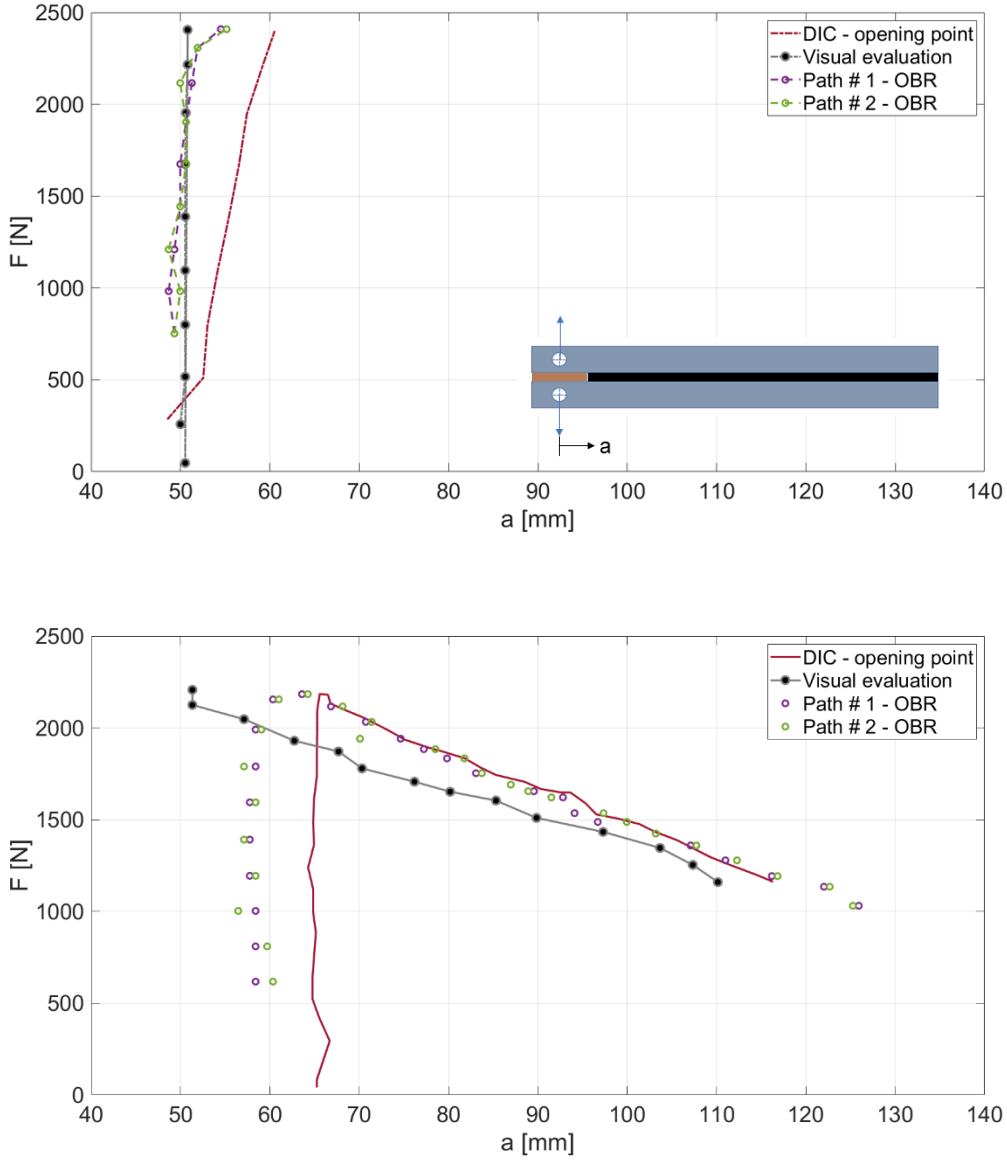

Figure 15: Comparison between the results obtained by the different techniques during (a) pre-cracking and (b) testing stage - specimen S2.

During the pre-cracking stage of specimen S1, a good agreement between the position of OBR strain peaks, DIC opening and visual evaluation of the crack tip was found. Their position remained fixed and equal to the position of the Teflon patch (50 mm) up to 1400 N, then moved towards slightly higher values of *a*, until the end of the pre-cracking stage.

In specimen S2, a good agreement was found between the position of the OBR strain peaks and the position of the crack tip identified visually, which remained almost equal to the initial 50 mm (position of the initial patch). In contrast, the position of the DIC opening gradually increased to 60 mm. This difference between the DIC outputs during the pre-cracking stage of both samples can be explained by an adhesive fracture surface observed at the beginning of sample S1 pre-cracking stage.

After unloading and during the successive test phase, for both specimens S1 and S2, it was observed that:

- when the load increases, up to the load peak, the positions of the OBR peaks and the crack tip detected by visual inspection remain almost equal to those reached after pre-cracking, whereas the DIC opening gradually increases;
- once the peak load is passed, it can be observed that the position of the DIC opening keeps travelling ahead of the crack tip, while the OBR peak positions are always comprised between the DIC opening and the crack tip detected visually. In specimen S2, the position of the OBR peaks and DIC opening point almost coincided.

Both observations agree with the existence of a process zone between the DIC opening and the crack tip. In addition, in both cases, the OBR strain peaks tend to be closer to the DIC opening points than crack tips. Finally, it is worth mentioning that in specimen S2, equipped with three optical fibre's paths, minor variations in each path's maximum strain peak values (approximately ± 2 mm) were recorded. However, it was not possible to infer a curvature of the crack front because the relative positions of the strain peaks changed during the propagation. In specimen S1, equipped with a single path on each adherend, no significant differences between the strain measurements on both sides of the substrates (upper and bottom part of the sample) were found.

For the present case of a thick metal DCB the simplest configuration with a single path is appropriate because the crack front is likely to remain straight. However, multiple paths can give additional information about the crack front for thin composite or hybrid

adhesively bonded joints like in ref [26], where a curved propagation front is more probable to occur; this layout should be preferred.

The direct comparison between the DIC opening points, visual evaluation positions and the OBR peaks for both specimens is reported in Figure 16.

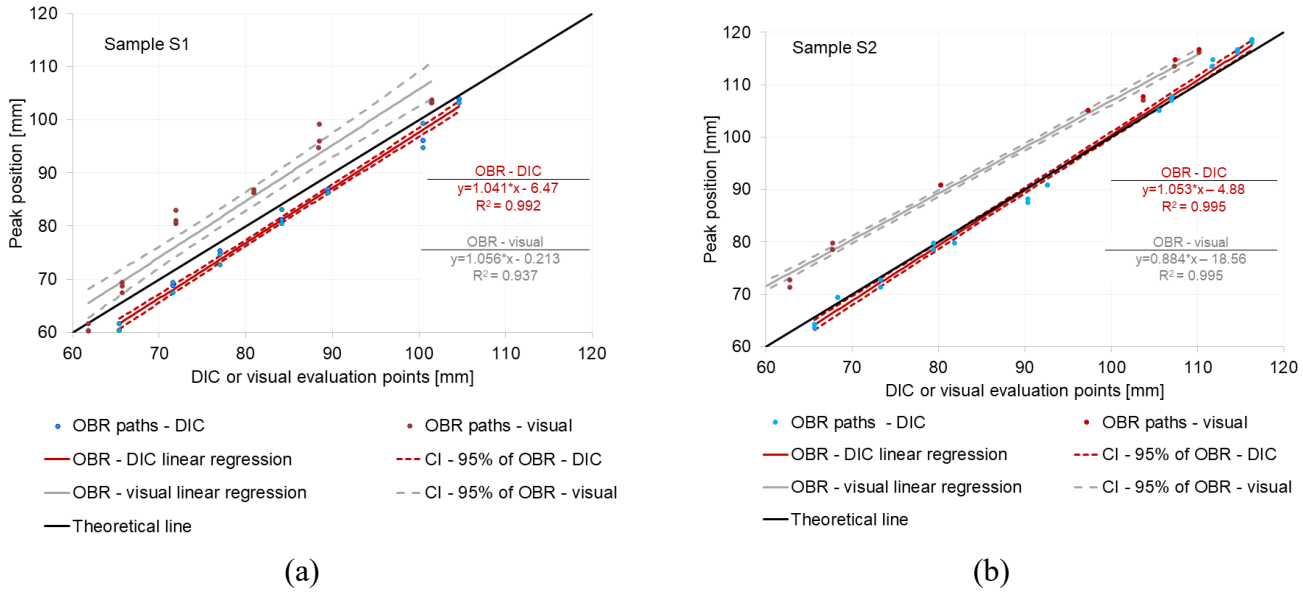

Figure 16: Comparison of the peak position and the crack length measured by the DIC and visual inspection during the testing stage for (a) specimen S1 and (b) specimen S2, with their respective confidence intervals (CI – 95%).

Figure 16 showcases the confidence analysis of the correlation of OBR data (positions of the strain peak) to DIC opening points (red curves) and the visual evaluation of the position of the crack tip (grey curves). The confidence bands associated with DIC and visual evaluation do not intersect for both specimens, meaning that both data sets are statistically different. However, the curve interpolating OBR data on DIC opening points falls close to the theoretical line oriented at 45° for both specimens, indicating that the position of the strain peak identified by the OBR method matches well that of the DIC opening point. For specimen S1, the average vertical offset between the theoretical and the interpolating line

is around 3 mm, whereas for S2 the vertical offset is negligible. Conversely, for both specimen S1 and S2, a much larger vertical offset characterizes the interpolating lines of OBR data on visual evaluation of the crack tip. This indicates that the position of the strain peak identified by the OBR method matches the DIC opening point better than the crack tip position. Therefore, for the studied adhesive and in a condition of cohesive failure, the strain peak position acquired by OBR is able to identify the onset of plasticisation of the adhesive instead of the crack tip position, i.e. the adhesive fracture.

Even when a not perfectly cohesive failure occurs (pre-cracking of specimen S1), the OBR strain peak position still falls in the region between the onset of the plasticisation determined by the DIC and the position of the completely fractured adhesive identified by visual evaluation. These results suggest that OBR back face strain measurements could identify damaged zones before any significant failure/fracture occurs, at least for adhesives with similar ductile behaviour as that of the one studied here and in the same loading conditions.

Future work will focus on fatigue loading and different loading modes and joints. In fatigue loading, a smaller cyclic plastic zone is expected and therefore, it is needed to check if the OBR method is still capable of identifying the onset of plasticity. As for loading modes and joints, in this work tests were conducted using the DCB specimen, which proves to be an excellent scientific tool, but it is far from a real joint. Therefore, the response of the OBR method in mode II, mixed-mode and real structural joints needs to be investigated before a reliable structural health monitoring system based on OBR back face distributed strain measurements could be proposed.

4. CONCLUDING REMARKS

The feasibility of applying OBR as a backface strain profile measurement tool of adhesive bonded double cantilever beams was investigated in this work. The obtained results were compared with DIC and visual inspection. As a result, the following conclusions can be drawn:

- The opening point identified using DIC as suggested in [44], i.e. the position where the transition between constant and variable relative vertical displacement between the adherents takes place, in the case of adhesively bonded DCB joints, for the particular adhesive studied in this work, corresponds to the onset of plasticisation of the adhesive and not to the crack-tip position;
- During crack propagation, the position of strain peaks recorded by OBR agrees with that of the DIC opening point; this suggests that an OBR backface strain method can identify the onset of the damage process zone in the adhesive rather than the crack tip position; although the size of the damage process zone cannot be determined, this feature is very attractive for the application of this technique as an experimental and in-service measuring approach because the onset of adhesive damage happens earlier than its final failure (fracture);
- Between DIC and OBR, the second appears to be more suitable for in-service damage measurement of bonded joints outside a laboratory; DIC, mainly due to the bulky equipment required, is likely to remain confined into the laboratory.

5. ACKNOWLEDGEMENT

Support by the Italian Ministry for Education, University and Research through the project Department of Excellence LIS4.0 (Integrated Laboratory for Lightweight e Smart Structures) is acknowledged.

We kindly thank Mr. Pablo Barriga Ruiz for the support in the execution of the experimental activities using DIC.

REFERENCES

[1] Ali M. T., Jumel J., Shanahan M. E. R. Effect of adhesion defects on crack propagation in double cantilever beam test. Int. J. Adhes. Adhes., **2018**, v. 84, 420–430. Doi: 10.1016/j.ijadhadh.2018.05.008.

[2] Srivastava V. K., Gries T., Quadflieg T., Mohr B., Kolloch M., Kumara P. Fracture behavior of adhesively bonded carbon fabric composite plates with nano materials filled polymer matrix under DCB, ENF and SLS tests. Eng. Fract. Mech., **2018**, v. 202, 275–287. Doi: 10.1016/j.engfracmech.2018.09.030.

[3] Costa M., Carbas R., Marques E., Viana G., da Silva L. F. M. An apparatus for mixed-mode fracture characterisation of adhesive joints. Theor. Appl. Fract. Mech., **2017**, v.91, 94–102. Doi: 10.1016/j.tafmec.2017.04.014.

[4] Hasegawa K., Crocombe A. D., Coppuck F., Jewel D., Maher S. Characterising bonded joints with a thick and flexible adhesive layer–Part 1: Fracture testing and behaviour. Int. J. Adhes. Adhes., **2015**, v. 63, 124–131. Doi: 10.1016/j.ijadhadh.2015.09.003.

[5] Salem N. B., Budzik M. K., Jumel J., Shanahan M. E. R., Lavelle F. Investigation of the crack front process zone in the Double Cantilever Beam test with backface strain monitoring technique. Eng. Fract. Mech., **2013**, v. 98, 272–283. Doi: 10.1016/j.engfracmech.2012.09.028.

[6] Grandt, A. F. Fundamentals of Structural Integrity: Damage Tolerant Design and Non-destructive Evaluation. Hoboken, N.J.: J. Wiley, 2003.

[7] Balageas D., Fritzen C. P., Güemes A. Structural Health Monitoring. J. Wiley, 2006.

[8] Huston D. Structural Sensing, Health Monitoring, and Performance Evaluation. J. Taylor & Francis Ltd, 2019.

[9] Quaegebeur N., Micheau P., Masson P., Castaings M. Methodology for optimal configuration in structural health monitoring of composite bonded joints. Smart Mater. Struct., **2012**, v.21. Doi: 10.1088/0964-1726/21/10/105001.

[10] Banea M. D., da Silva L. F. M. Adhesively bonded joints in composite materials: an overview. J. Mater.: Des. Appl., **2009**, vol. 223. Doi: 10.1243/14644207JMDA219.

[11] Weiland J., Sadeghi M. Z., Thomalla J. V., Schiebahn A., Schroeder K. U., Reisgen U. Analysis of backface strain measurement for adhesively bonded single lap joints using strain gauge, Digital Image Correlation, and finite element method. Int. J. Adhes. Adhes., **2020**, v. 97. Doi: 10.1016/j.ijadhadh.2019.102491.

[12] Alnuaimi H., Amjad U., Russo P., Lopresto V., and Kundu T. Monitoring damage in composite plates from crack initiation to macrocrack propagation combining linear and non-linear ultrasonic techniques. Struct. Health Monit., **2020**. Doi: 10.1177/1475921720922922.

[13] Droubi M. G., Stuart A., Mowat J., Noble C., Prathuru A. K., Faisal N. H. Acoustic emission method to study fracture (Mode-I, II) and residual strength characteristics in composite-to-metal and metal-to-metal adhesively bonded joints. J. Adhes., **2018**, v.94, 347-386. Doi: 10.1080/00218464.2017.1278696.

[14] Bernasconi A., Kharshiduzzaman M. D., Comolli L. Strain Profile Measurement for Structural Health Monitoring of Woven Carbon-fiber Reinforced Polymer Composite Bonded joints by Fiber Optic Sensing Using an Optical Backscatter Reflectometer. J. Adhes., **2016**, v.96, 440-458. Doi: 10.1080/00218464.2015.1043005.

[15] Shenoy V., Ashcroft I. A., Critchlow G. W., Crocombe A. D., Abdel Wahab M. M. An investigation into the crack initiation and propagation behaviour of bonded single lap joints using backface strain. Int. J. Adhes. Adhes., **2009**, v. 29, 361-371. Doi: 10.1016/j.ijadhadh.2008.07.008.

[16] Sadeghi M. Z., Weiland J., Preisler A., Zimmermann J., Schiebahn A., Reisgen U., Schroeder K. U. Damage detection in adhesively bonded single lap joints by using backface strain: proposing a new position for backface strain gauges. Int. J. Adhes. Adhes., **2020,** v. 97. Doi: 10.1016/j.ijadhadh.2019.102491.

[17] Bernasconi A., Comolli L. An investigation of the crack propagation in a carbon fiber bonded joint using backface strain measurements with FBG sensors. Int. Conf. Optical Fiber Sensor, **2012**, v.22. Doi: 10.1117/12.975143.

[18] Pereira G., Mikkelsen L., Mcgugan M. Monitoring the failure forms of a composite laminate system by using panda polarisation maintaining fiber Bragg gratings. Opt. Laser Technol., **2015**, pp. 133-139. Doi: 10.1364/OE.27.017571.

[19] Chunsheng S., Jiaxiang Z., Mo Y., Erwei S., Jinguang Z. Reconstruction of fiber Bragg grating strain profile used to monitor the stiffness degradation of the adhesive layer in carbon fiber–reinforced plastic single-lap joint. Adv. Mech. Eng., **2017**, v.9. Doi: 10.1177/1687814016688575.

[20] Peairs, D.M.; Sterner, L.; Flanagan, K.; Kochergin, V. Fiber optic monitoring of structural composites using optical backscatter reflectometry. In Proceedings of the 41st Int. SAMPE Technol. Conf., Wichita, KS, USA, 19–22 October **2009**.

[21] Guemes A., Lopez A. F., Soller B. Optical Fiber Distributed Sensing - Physical Principles and Applications. Struct. Health Monit., **2010**, v.9, 233-13. Doi: 10.1177/1475921710365263.

[22] Lomperski S., Gerardi C., Pointer W. D. Fiber optic distributed temperature sensor mapping of a jet-mixing flow field. Exp. Fluids, **2015**, 56:55. Doi: 10.1007/s00348-015-1918-6.

[23] Grave J. H. L., Håheim M. L., Echtermeyer A. T. Evaluation of the strain field in a composite – metal adhesive joint with an optical backscatter reflectometer. ECCM 15, **2015**.

[24] Bernasconi A., Carboni M., Comolli L., Galeazzi R., Gianneo A., Kharshiduzzaman M. D., Fatigue Crack Growth Monitoring in Composite Bonded Lap Joints by a Distributed Fibre Optic Sensing System and Comparison with Ultrasonic Testing. J. Adhes., **2016**, v.92. Doi: 10.1080/00218464.2015.1123153.

[25] Grave J. H. L., Håheim M. L., Echtermeyer A. T. Measuring changing strain fields in composites with Distributed Fiber-Optic Sensing using the optical backscatter reflectometer. Composites Part B, **2015**, v. 74, 138 – 146. Doi: 10.1016/j.compositesb.2015.01.003.

[26] Truong H.T.X., Martinez M.J., Ochoa O.O., Lagoudas D.C., Mode I fracture toughness of hybrid co-cured Al-CFRP and NiTi-CFRP interfaces: An experimental and computational study, Composites Part A, 2020 (135), 105925, doi.org/10.1016/j.compositesa.2020.105925.

[27] Mudassar A. A., Butt S. Improved Digital Image Correlation method. Opt. Lasers Eng., **2016**, v. 87, 156–167. Doi: 10.1016/j.optlaseng.2015.10.002.

[28] Yoneyama S., Morimoto Y., Takashi M. Automatic Evaluation of Mixed-mode Stress Intensity Factors Utilising Digital Image Correlation. Strain, **2006**, v. 42, 21 – 29. Doi: 10.1111/j.1475-1305.2006. 00246.x.

[29] Blaysat B., Hoefnagels J. P. M., Lubineau G., Alfano M., Geers M. G. D. Interface debonding characterisation by image correlation integrated with Double Cantilever Beam kinematics. Int. J. Solids Struct., **2015**, v.55, 79 – 91. Doi: 10.1016/j.ijsolstr.2014.06.012.

[30] Budhea S., Banea M. D., Barrosa S. de, da Silva L. F. M. Digital image correlation strain measurement of thick adherend shear test specimen joined with an epoxy film adhesive. Int. J. Adhes. Adhes., **2017,** v. 72, 30-42. Doi: 10.1016/j.ijadhadh.2016.10.010.

[31] Gorman J. M., Thouless M. D. The use of digital-image correlation to investigate the cohesive zone in a double-cantilever beam, with comparisons to numerical and analytical models. J. Mech. Phys. Solids, **2019**, v. 123, 315-331. Doi: 10.1016/j.jmps.2018.08.013.

[32] Reiner J., Torres J. P., Veidt M. A novel Top Surface Analysis method for Mode I interface characterisation using Digital Image Correlation. Eng. Fract. Mech., **2017**, v.173, 107 – 117. Doi: 10.1016/j.engfracmech.2016.12.022.

[33] Shen B., Paulino G. H. Direct Extraction of Cohesive Fracture Properties from Digital Image Correlation: A Hybrid Inverse Technique. Exp. Mech., **2011**, v.51, 143–163. Doi: 10.1007/s11340-010-9342-6.

[34] Richter-Trummer V., Marques E. A., Chaves F. J. P., Tavares J. M. R. S., da Silva L. F. M., de Castro P. M. S. T. Analysis of crack growth behavior in a double cantilever beam adhesive fracture test by different digital image processing techniques. Mat.-wiss. u. Werkstofftech., **2011**, v. 42, 452 – 459. Doi: 10.1002/mawe.201100807.

[35] Hoult N. A., Take W. A., Lee C., Dutton M. Experimental accuracy of two-dimensional strain measurements using Digital Image Correlation. Eng. Struct., **2013**, v.46, 718–726. Doi: 10.1016/j.engstruct.2012.08.018.

[36] Chernyatin A. S., Matvienko Y. G., Lopez-Crespo P. Mathematical and numerical correction of the DIC displacements for determination of stress field along crack front. Procedia Struct. Integrity, **2016**, v.2, 2650–2658. Doi: 10.1016/j.prostr.2016.06.331.

[37] Thäsler T., Holtmannspötter, J, Gudladt, H.-J. Monitoring the fatigue crack growth behavior of composite joints using in situ 2D-digital image correlation, J. Adhes., 2019, 95:5-7, 595-613, DOI: 10.1080/00218464.2018.1562923

[38] Bernasconi A., Lima R. A. A., Cardamone S., Campbell R. B., Slocum A. H., Giglio M. Effect of temperature on cohesive modelling of 3M Scotch-Weld™ 7260 B/A epoxy adhesive. J. Adhes., **2019**. Doi: 10.1080/00218464.2019.1665519.

[39] Cardamone S., Bernasconi A., Giglio M. Characterization of the 3M Scotch-Weld™ 7260 B/A epoxy adhesive by cohesive damage models and application to a full-scale bonded sub-structure. J. Adhes., **2019**. Doi: 10.1080/00218464.2019.1591278.

[40] American Society for Testing and Materials International, “ASTM D3433-99, Standard Test Method for Fracture Strength in Cleavage of Adhesives in Bonded Metal Joints,” West Conshohocken, **2012**.

[41] International Organization for Standardization (ISO), “ISO 25217, Adhesives — Determination of the mode 1 adhesive fracture energy of structural adhesive joints using double cantilever beam and tapered double cantilever beam specimens,” Geneva, **2009**.

[42] Barrias A., Casas J. R., Villalba S. Distributed optical fibre sensors in concrete structures: Performance of bonding adhesives and influence of spatial resolution. Struct. Control Health Monit., **2019**, v. 26. Doi: 10.1002/stc.2310.

[43] Saha S., Sullivan R. W. Strain distributions in bonded composites using optical fibers and digital image correlation. American Society for Composites, **2019**. Doi: 10.12783/asc34/31415.

[44] Zhu M., Gorbatikh L., Fonteyn S., Van Hemelrijck D., Pyl L., Carrella-Payan D., Lomov S. V. Digital image correlation assisted characterisation of mode I fatigue delamination in composites. J. Comp. Struct., 2020, v. 253. Doi : 10.1016/j.compstruct.2020.112746.

[45] Morais J. J. L., de Moura M. F. S. F., Pereira F. A. M., Xavier J., Dourado N., Dias M. I. R., Azevedo J. M. T. The double cantilever beam test applied to mode I fracture characterisation of cortical bone tissue. J. Mech. Behav. Biomed. Mater., **2010**, 446-453. Doi: 10.1016/j.jmbbm.2010.04.001.